Karlo Seleš[1], Zdenko Tonković[1], Ante Jurčević[1], Jurica Sorić[1]

Numerical Modelling of Fracture Processes at the Microstructural level of Heterogeneous Materials

[1]Faculty of Mechanical Engineering and Naval Architecture, University of Zagreb, Zagreb, Croatia

Abstract

The prediction of a crack propagation at the microstructural level of heterogeneous material, as is the case with the nodular cast iron, can be a very demanding problem. Lately, the phase-field approach to fracture has been shown a strong potential in modelling such complex crack behaviour in a smeared-crack manner. In this work, the phase-field staggered residual norm based stopping criterion, recently developed by the authors, has been utilized for the numerical simulation of the crack propagation within the heterogeneous microstructural geometry. The geometries have been based on the metallographic images of the nodular cast iron with the graphite nodules considered as porosities. The proposed solution strategy is able to recover the complicated crack nucleation and propagation phenomena within the complex microstructural topology.

Keywords: heterogeneous materials, phase-field fracture modelling, staggered algorithm, Abaqus, crack initiation and propagation.

1. Introduction

An accurate deformation response analysis of the heterogeneous materials often demands a precise modelling at both macroscopic and microscopic scales. The nodular cast iron is a good example of the material with highly heterogeneous microstructure consisting of graphite nodules placed inside a ferritic or a pearlitic matrix. However, not only the volume fraction and the material properties of the microstructural constituents, but also their size, shape and spatial distribution has an important influence on the macroscopic material behaviour, as was presented in [1]. The experimental observations of the ductile nodular cast iron EN-GJS-400-18-LT mechanical behaviour, with emphasis on its material microstructure, have been well described in the previous works of the authors' research team [2, 3]. The cracked specimen with exposed nodular cast iron microstructure is presented in Fig. 1 where it can be seen how the crack is directed towards the graphite nodule which then acts as a barrier for further crack propagation. This is part of the reason why the nodular cast iron has great material fatigue properties and is often used in engineering practice for the design of the structural components subjected to the cyclic loads.
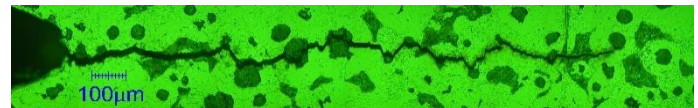
Fig. 1. Microstructural crack exposure [3]

Such cracking behaviour within the heterogeneous microstructure is often consisted of complex cracking mechanisms such as the crack initiation and propagation, accompanied with the branching and merging of the crack paths. As a consequence, numerical modelling of fracture processes in heterogeneous microstructure poses an important and a challenging problem. Accordingly, different numerical approaches and methods have been proposed for material fracture modelling. Often used numerical methods, which can be classified as the discrete crack interface methods for material fracture, introduce the crack as a geometric discontinuity within the finite element framework. However, such methods are generally known to suffer from the mesh-density and direction dependence problem as the crack propagation usually occurs along the element edges. This problem has been successfully solved via the automatic remeshing [4] or enriching the standard finite element shape functions through a partition of unity method (XFEM) [5], thus making the methods easily applicable in modelling the crack propagation and their use widespread. Such discrete crack modelling methods are still not without the problems as they often lack computational efficiency, especially in three-dimensional computations, or provide spurious damage growth and incorrect solutions when dealing with complex fracture phenomena.

On the other hand, the so-called diffusive crack modeling approaches approximate the crack discontinuity by smearing it over the finite volume domain. Such regularization is often controlled by some length-scale parameter. In recent years, a phase-field method which can also be categorized as the diffusive crack modeling approach, has gained a great popularity in modelling the crack propagation phenomena. It has been developed from the variational approach to fracture [6], thus recasting the original Griffith's fracture theory to the energy minimization problem. It introduces a scalar field (called the phase-field parameter) which can be physically interpreted as the damage variable that continuously varies over the domain between the fully broken and intact material phases. The need to numerically track the displacement field discontinuities is thus averted. In addition, the method is variationally and thermodynamically consistent, and thus no ad hoc criteria are needed to solve the complex fracture processes including the aforementioned crack nucleation, propagation, merging or branching, which significantly simplifies its numerical implementation even in three-dimensional settings, as has been shown in [7-9]. Nevertheless, it can often be computationally demanding due to the very fine mesh requirement imposed by the aforementioned length-scale parameter. Over the recent years, a great number of studies has been done on the phase-field brittle fracture modeling of homogeneous isotropic media [10-12]. A great overview of the phase-field brittle fracture models is provided in [13].

The phase-field fracture models are more commonly implemented via the robust staggered system approach, because the pure monolithic approaches suffer from the numerical instabilities as a results of the non-convexity of the initial phase-field free energy functional with respect to the phase-field and displacement field [14]. The staggered algorithms uncouple the system of equations to solve it in an incremental-iterative manner [11]. As their efficiency and convergence rate are influenced by the choice of the stopping criterion within the iterative scheme, different stopping criteria have been used, e.g., the normalized change of the system's energy [13] or the successive iteration solution error [9, 14].

The importance of the stopping criterion use was presented in the authors' recent work [15] where the Abaqus [16] implementation of the staggered algorithm with the stopping criterion based on the residual norm control [17] is provided.

In this paper, the use of this algorithm is demonstrated on the heterogeneous microstructure fracture analysis. It should be stressed that the phase-field modelling of the fracture processes occurring at microlevel of heterogeneous materials have been the subject of current research activities in scientific community [18] with many open questions and unresolved issues.

The paper is structured as follows. A brief overview of the phase-field approach to fracture is presented in Section 2. The numerical implementation of the model presented in the authors' former work [15] is outlined in Section 3. The numerical simulations of the fracture process on the simplified microstructural geometry of nodular cast iron are presented in Section 4. Finally, the concluding remarks are drawn in Section 5.

2. Phase-field fracture formulation

Let us consider an elastic *n*-dimensional body Ω with crack surface $\Gamma(t)$ as presented in Fig. 2.
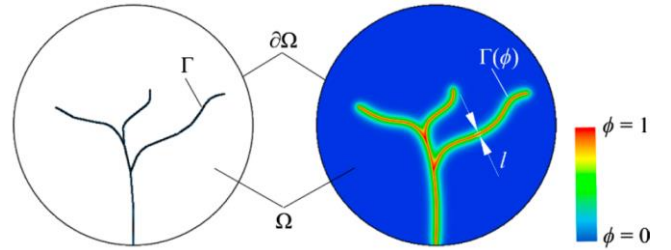
Fig. 2. Elastic *n*-dimensional body Ω with a discrete (left) and diffusive crack surface (right) [15]

The phase-field fracture approach is then governed by a minimization problem of the free energy functional

$$\Psi = \Psi^b + \Psi^s = \int_{\Omega/\Gamma} \psi_e(\boldsymbol{\varepsilon}) d\Omega + \int_{\Gamma} G_c d\Gamma, \qquad (1)$$

where Ψ^b represents the elastic deformation energy, while Ψ^s is the dissipated fracture surface energy. $\boldsymbol{\varepsilon}$ is the small strain tensor, while G_c stands for the fracture toughness. The dissipated fracture energy corresponds to the creation of new surfaces upon the onset of cracking. It can be seen as an extension of the Griffith's fracture theory [13], where a material fails upon reaching the critical value of the

fracture toughness G_c. In Eq. (1), ψ_e is the elastic strain-energy density function formulated as

$$\psi_e = \tfrac{1}{2}\lambda \mathrm{tr}^2\left(\boldsymbol{\varepsilon}\right) + \mu\mathrm{tr}\left(\boldsymbol{\varepsilon}^2\right) \qquad (2)$$

with the Láme constants λ and μ. In the presented regularized framework, the crack geometry is approximated by a smeared representation defined by a scalar phase-field parameter $\phi \in [0,1]$, which takes value of 1 for the fully broken material state and the value of 0 for the bulk material (Fig. 2), thus restating the fracture energy Ψ^s over the volume domain. Accordingly, the elastic deformation energy part Ψ^b is regularized by the introduction of a degradation function $(1-\phi)^2$ to account for the subsequent loss of stiffness in the region representing the diffusive crack (i.e. $\phi \rightarrow 1$). The regularized free energy functional can then be written as

$$\Psi\left(\mathbf{u},\phi\right) = \int_\Omega \left(1-\phi\right)^2 \psi_e\left(\boldsymbol{\varepsilon}\right)\mathrm{d}\Omega + \int_\Omega \frac{G_c}{2}\left[l\left(\nabla\phi\right)^2 + \frac{1}{l}\phi^2\right]\mathrm{d}\Omega, (3)$$

where l is the length scale parameter that regulates the width of the crack band approximation, while $\mathbf{u}$ denotes the displacement field. Furthermore, the crack irreversibility is introduced via the history field $\mathrm{H}(t) := \max_{\tau=[0,t]} \psi_e(\tau)$ [8] which thus substitutes ψ_e and prevents the crack "healing". Governing equations are obtained using the principle of virtual work and can be written as follows

$$\begin{aligned}
&\nabla\boldsymbol{\sigma} + \bar{\mathbf{b}} = 0 \quad \text{in } \Omega, \\
&\boldsymbol{\sigma}\cdot\mathbf{n} = \bar{\mathbf{t}} \quad \text{on } \partial\Omega_{\bar{t}}, \\
&\mathbf{u} = \bar{\mathbf{u}} \quad \text{on } \partial\Omega_{\bar{u}}, \\
&-G_c l\Delta\phi + \left[\frac{G_c}{l} + 2\psi_e^+\right]\phi = 2\psi_e^+ \quad \text{in } \Omega, \\
&\nabla\phi\cdot\mathbf{n} = 0 \quad \text{on } \partial\Omega,
\end{aligned} \qquad (4)$$

where $\bar{\mathbf{b}}$ and $\bar{\mathbf{t}}$ are the prescribed volume and surface forces, $\bar{\mathbf{u}}$ is the prescribed displacement, $\mathbf{n}$ is the normal vector on the boundary $\partial\Omega$, and $\boldsymbol{\sigma} = \dfrac{\partial\psi}{\partial\boldsymbol{\varepsilon}}$ is the Cauchy stress. Detailed information on the phase-field fracture formulation can be found in [10].

3. Numerical implementation

The phase-field formulation is implemented into the finite element framework by means of the four-node plane strain element with the standard displacement degrees of freedom and the phase-field parameter ϕ as an additional degree of freedom at each node. The same shape functions are applied to interpolate both fields, ϕ and $\mathbf{u}$. Finally, in accordance with the staggered solution scheme, the decoupled system of equations is obtained as follows

$$\begin{aligned}
\mathbf{K}^{\phi\phi}\phi &= \mathbf{R}^\phi\left(\mathbf{u},\phi\right), \\[4pt]
\mathbf{K}^{\mathbf{uu}}\mathbf{u} &= \mathbf{R}^{\mathbf{u}}\left(\mathbf{u},\phi\right),
\end{aligned} \qquad (5)$$

where $\mathbf{K}^{\mathbf{uu}}$ and $\mathbf{K}^{\phi\phi}$ are stiffness matrices, while $\mathbf{R}^{\mathbf{u}}$ and $\mathbf{R}^\phi$ are residual force vectors corresponding to the degrees of freedom $\mathbf{u}$ and ϕ, expressed as

$$\mathbf{R}_i^{\mathbf{u}} = \int_\Omega \mathbf{B}_i^{\mathbf{u}^T}\boldsymbol{\sigma}\,\mathrm{d}\Omega - \int_\Omega \mathbf{N}_i^{\mathbf{u}^T}\bar{\mathbf{b}}\,\mathrm{d}\Omega - \int_{\partial\Omega}\mathbf{N}_i^{\mathbf{u}^T}\bar{\mathbf{t}}\,\mathrm{d}\partial\Omega,$$
$$(6)$$
$$\mathbf{R}_i^\phi = \int_\Omega \left\{ G_c l\mathbf{B}_i^{\phi^T}\nabla\phi + \left[\frac{G_c}{l} + 2\mathrm{H}\right]\mathbf{N}_i^\phi\phi - 2\mathbf{N}_i^\phi\mathrm{H}\right\}\mathrm{d}\Omega,$$

and

$$\frac{\partial\mathbf{R}_i^u}{\partial\mathbf{u}_j} = \mathbf{K}_{ij}^{\mathbf{uu}} = \int_\Omega \mathbf{B}_i^{\mathbf{u}^T}\frac{\partial\boldsymbol{\sigma}}{\partial\boldsymbol{\varepsilon}}\mathbf{B}_j^{\mathbf{u}}\mathrm{d}\Omega,$$
$$(7)$$
$$\frac{\partial\mathbf{R}_i^\phi}{\partial\phi_j} = \mathbf{K}_{ij}^{\phi\phi} = \int_\Omega \left\{ G_c l\mathbf{B}_i^{\phi^T}\mathbf{B}_j^\phi + \left[\frac{G_c}{l} + 2\mathrm{H}\right]\mathbf{N}_i^\phi\mathbf{N}_j^\phi\right\}\mathrm{d}\Omega.$$

In the above equations, $\mathbf{B}$ denotes the displacement differentiation matrix, while $\mathbf{N}$ stands for the shape function matrix. Fig. 3 shows the flowchart of the staggered algorithm implemented in the FE software Abaqus [16] via the layered user element system generated by UEL and UMAT subroutines. The flowchart corresponds to the updated version of the algorithm [17] which is openly accessible on Mendeley repository. For more information on the updated version, see [17].
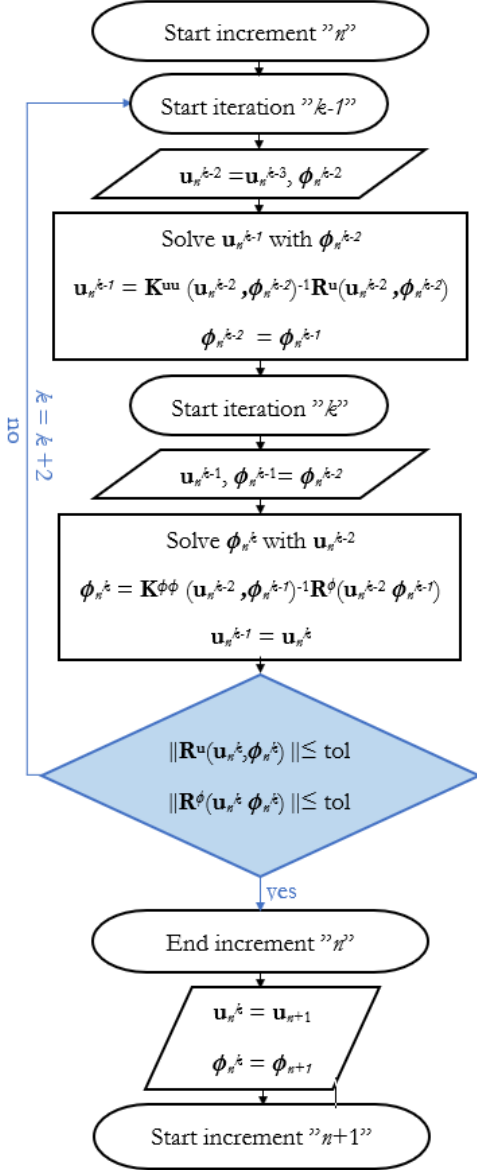
Fig. 3. RCTRL staggered algorithm flowchart [17]

Here, the solution estimates ϕ_n^k and $\mathbf{u}_n^k$ are obtained by the Newton-Raphson procedure after the non-converging iteration as follows

$$\phi_n^k = \phi_n^{k-1} + \mathbf{K}^{\phi\phi}\left(\mathbf{u}_n^{k-2}, \phi_n^{k-1}\right)^{-1} \mathbf{R}^{\phi}\left(\mathbf{u}_n^{k-2}, \phi_n^{k-1}\right),$$

$$(8)$$

$$\mathbf{u}_n^k = \mathbf{u}_n^{k-1} + \mathbf{K}^{\mathbf{uu}}\left(\mathbf{u}_n^{k-1}, \phi_n^{k-1}\right)^{-1} \mathbf{R}^{\mathbf{u}}\left(\mathbf{u}_n^{k-1}, \phi_n^{k-1}\right).$$

For more details on the numerical implementation, see [15, 20]. The presented phase-field approach has been evaluated and verified on standard benchmark examples in [15] and on the problems of real microstructural geometries in [20], in comparison with the common single iteration staggered algorithm [11]. Here, its capability has been demonstrated through the simulation of the fracture phenomena occurring on the microstructural geometry of the nodular cast iron by the numerical example elaborated in the next section.

4. Numerical examples

The performance of the algorithm is tested on the numerical examples of homogeneous plate subjected to tensile loading and the heterogeneous microstructural geometries.

Homogeneous plate example
A homogeneous 1×1 mm plate is discretized by one element as presented in Fig. 4 and subjected to tension. Since the analytical solution is known for this setup, this example is widely used as a test case in the literature, e.g. in [21]. The material properties are chosen as follows: the Young's modulus $E = 210$ kN/mm^2, Poisson's ratio $v = 0.3$ and critical fracture energy density $G_c = 2.7 \times 10^{-3}$ kN/mm. The length scale parameter is set to $l = 2$ mm. The analytical solution

$$\phi = \frac{C\varepsilon_x^2}{\dfrac{G_c}{l} + C\varepsilon_x^2} \qquad (9)$$

is obtained from Eq. (3) setting the crack surface gradient to zero, corresponding to the homogeneous case $(\nabla\phi = 0)$. Thus, the axial stress can be calculated as $\sigma = (1-\phi)^2 C\varepsilon$.
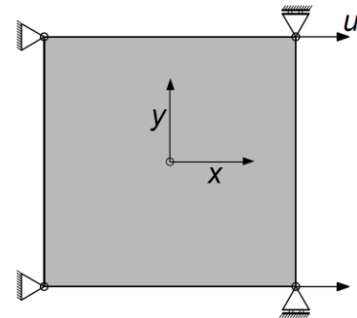
Fig. 4. Geometry and boundary conditions of the homogeneous plate subjected to tension [15]

The example is solved using 4 different loading increments Δu to reach $u = 0.01$ mm, namely $\Delta u = 2.5 \times 10^{-3}$ mm, $\Delta u = 5 \times 10^{-3}$ mm, $\Delta u = 1 \times 10^{-3}$ mm and $\Delta u = 1 \times 10^{-4}$ mm. The

axial stress-strain response comparison of the residual control staggered algorithm against the analytical solution is presented in Fig. 5. It can be seen that the algorithm matches well with the analytical solution even for large loading increments which is not the case for the staggered algorithms without the iterative loop, as tested in [15].
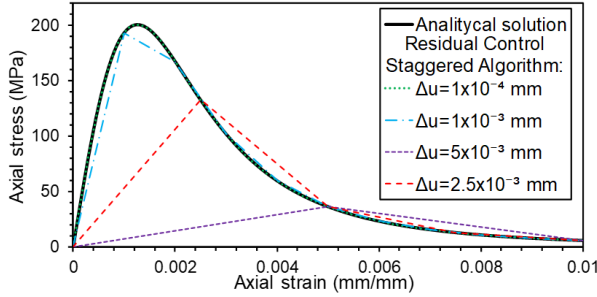
Fig. 5. Stress-strain curves obtained by the residual control staggered algorithm in comparison with the analytical solution.

Heterogeneous microstructure fracture analysis
Fig. 6 shows the heterogeneous microstructure of the nodular cast iron grade EN-GJS-400-18-LT produced by the inmould casting technique and obtained by the metallography in the authors' research team previous work [2, 3]. This ductile nodular cast iron consists of graphite nodules surrounded by a ferritic matrix. For the considered material the volume fraction of graphite nodules is about 7% with circularity of 0.7 (where the value of 1.0 indicates a perfect circle). The academic brittle material properties are used to predict the brittle fracture nucleation and propagation because the present algorithm is not yet expanded to the ductile fracture problem at this moment. As a numerical idealization, the graphite nodules are substituted with spheres. In the considered 2D case, the spheres are projected as circles. Since the academic brittle material properties are already assumed, it seems justified to idealize the nodules as spheres, i.e., circles, to speed up the numerical simulations.

Twelve different microstructural samples or Microstructural Volume Elements (MVEs) are randomly selected from the metallographic image while still satisfying the average graphite nodules content of ~7%, as schematically shown in Fig. 6 and Table 1. The size of the samples is 161.7 x 161.7μm. The MVEs are uniformly discretized with ~30 000 finite elements with an average characteristic element length of $h = 0.001$ mm. The academic material properties are: Young's modulus $E =$

200 GPa, Poisson's ratio $v = 0.3$ and fracture toughness $G_c = 1 \times 10^3$ N/m. The regularizing parameter is set to $l = 0.0025$ mm. The displacement boundary conditions imposed on the MVE are presented in Fig. 7.
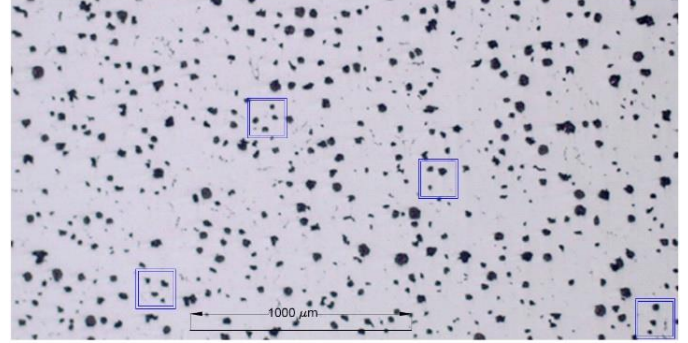
Fig. 6. Metallographic image of EN-GJS-400-18-LT microstructure [3] with the selection of samples satisfying the global average graphite nodules content

Table 1. Critical force for different samples under tensile loading

Serial number of MVE	Pore share, %	Critical force, N	Critical force deviation from average, %
1	6.19	282.9	4.16
2	6.53	250.5	7.76
3	5.94	290.0	6.78
4	6.30	282.3	3.94
5	6.74	261.3	3.79
6	6.11	254.4	6.33
7	6.39	281.7	3.72
8	6.21	285.9	5.27
9	6.24	263.9	2.83
10	6.01	276.1	1.66
11	6.30	277.6	2.21
12	6.11	252.5	7.03
Average	6.26	271.6	

The problem is solved with the proposed algorithm in the displacement-controlled regime. Fig. 8 presents crack paths in the simplified geometry of a nodular cast iron microstructure. As evident, the proposed phase-field formulation can successfully calculate the complicated crack paths on the heterogeneous microstructural geometry. The reaction force of the right edge of MVE versus the displacement diagrams for all considered MVEs are shown in Fig. 9.

Fig. 7. Displacement boundary conditions imposed on the MVE

MVE1   MVE2   MVE3

MVE4   MVE5   MVE6

MVE7   MVE8   MVE9

MVE10   MVE11   MVE12
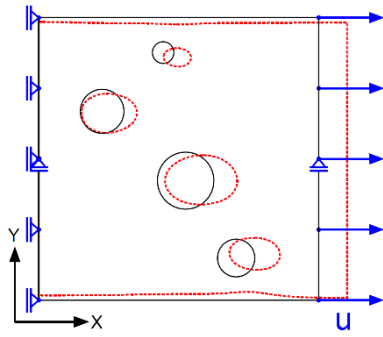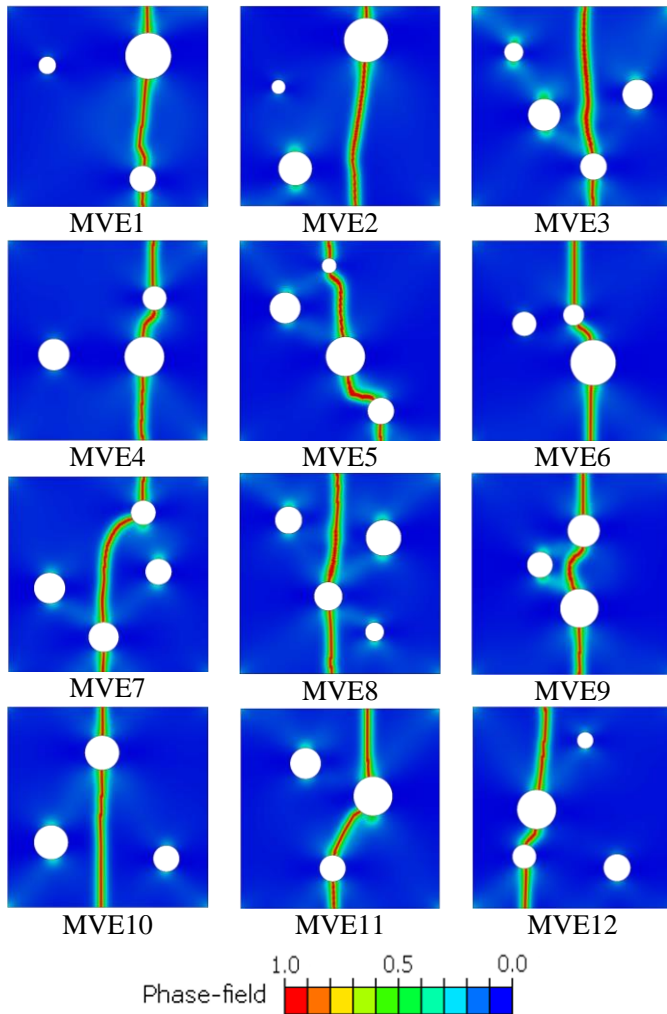
Fig. 8. Crack paths in the simplified geometry of a nodular cast iron microstructure

It is obvious that there is no significant difference in the post-peak behaviour of the specimens. In that area the force-displacement curves demonstrate a rapid drop in

stiffness after reaching a critical force value as a consequence of an abrupt crack propagation between the microstructural inclusions. Such crack propagation is typical for a class of brittle materials, which is in accordance with the assumptions established in this work. Furthermore, the maximum force and displacement are shown in Table 1.
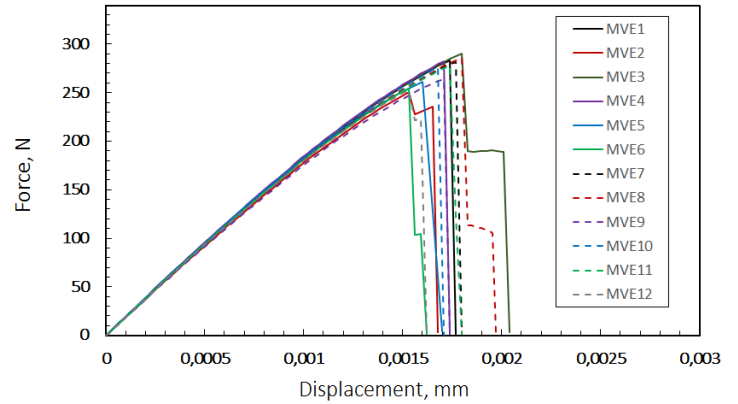
Fig. 9. Force-displacement response for all considered MVEs

5. Conclusions

The fracture analysis of the heterogeneous microstructural geometry based on the microstructural imaging of nodular cast iron has been performed in this paper. The phase-field staggered algorithm with residual norm based stopping criterion, recently developed as a part of author's previous study, has been utilized. The algorithm was implemented into the finite element program Abaqus by means of the custom linear quadrilateral finite elements with the phase-field parameter as an additional degree of freedom. The concise implementation details are presented together with the verification on the standard benchmark test as well as the demonstration of the model capabilities on the heterogeneous nodular cast iron microstructure represented by the series of MVEs. The obtained results display the ability of the model to capture the brittle crack initiation and propagation, resulting in complex crack paths on heterogeneous microstructural geometries. Although an academic brittle material was employed together with simplifications to geometry, it can still be observed that the maximal deviation of the critical force is not obtained on the MVEs with greatest deviation from average pore share,

which shows how the microstructural geometry arrangement also plays a significant role together with the porosity ratio. However, it has to be emphasized that the obtained results serve as a demonstration of the algorithms capabilities on complex heterogeneous microstructural geometries and, due to these simplifications, do not represent a realistic material behaviour.

References

[1] Hütter, G., Zybell, L., Kuna, M., Micromechanisms of fracture in nodular cast iron: From experimental findings towards modeling strategies – A review. *Eng Fract Mech.*, 144, 118–41 (2015).

[2] Čanžar, P., Tonković, Z., Kodvanj, J., Microstructure influence on fatigue behaviour of nodular cast iron. *Mater Sci Eng A*, 556, 88–99 (2012).

[3] Čanžar, P., Experimental and Numerical Modelling of Fatigue Behaviour of Nodular Cast Iron, Faculty of Mechanical Engineering and Naval Architecture, University of Zagreb, PhD Thesis, 2012 (in Croatian).

[4] Ingraffea, A.R., Saouma, V., Numerical modeling of discrete crack propagation in reinforced and plain concrete. In: Sih G.C., DiTommaso A. (eds) Fracture mechanics of concrete: Structural application and numerical calculation. Engineering Application of Fracture Mechanics, Dordrecht, Springer, 4 (1985).

[5] Moës, N., Dolbow, J., Belytschko, T., A finite element method for crack growth without remeshing. *Int. J. Numer. Methods Eng.*, 46(1), 131–150 (1999).

[6] Francfort, G.A., Marigo, J.J., Revisiting brittle fracture as an energy minimization problem. *Journal of the Mechanics and Physics of Solids*, 46(8), 1319-1342 (1998).

[7] Miehe, C., Aldakheel, F., Raina, A., Phase field modeling of ductile fracture at finite strains: A variational gradient-extended plasticity-damage theory. *International Journal of Plasticity*, 84, 1-32 (2016).

[8] Molnar, G., Gravouil, A., 2D and 3D Abaqus implementation of a robust staggered phase-field solution for modeling brittle fracture. *Finite Elements in Analysis and Design*, 130, 27-38 (2017).

[9] Zhou, S.W., Zhuang, X.Y., Zhu, H.H., Rabczuk, T., Phase field modelling of crack propagation, branching and coalescence in rocks. *Theoretical and Applied Fracture Mechanics*, 96, 174-192 (2018).

[10] Miehe, C., Welschinger, F., Hofacker, M., Thermodynamically consistent phase-field models of fracture: Variational principles and multi-field FE implementations. *International Journal for Numerical Methods in Engineering*, 83(10), 1273-1311 (2010).

[11] Miehe, C., Hofacker, M., Welschinger, F., A phase field model for rate-independent crack propagation: Robust algorithmic implementation based on operator splits. *Computer Methods in Applied Mechanics and Engineering*, 199(45-48), 2765-2778 (2010).

[12] Vignollet, J., May, S., de Borst, R., Verhoosel, C.V., Phase-field models for brittle and cohesive fracture. *Meccanica*, 49(11), 2587-2601 (2014).

[13] Ambati, M., Gerasimov, T., De Lorenzis, L., A review on phase-field models of brittle fracture and a new fast hybrid formulation. *Computational Mechanics*, 55(2), 383-405 (2015).

[14] Bourdin, B., Francfort, G.A., Marigo, J.J., The variational approach to fracture. *Journal of Elasticity*, 91(1-3), 5-148 (2008).

[15] Seleš, K., Lesičar, T., Tonković, Z., Sorić, J., A residual control staggered solution scheme for the phase-field modeling of brittle fracture. *Engineering Fracture Mechanics*, 205, 370-386 (2018).

[16] Abaqus 6.14-1, Dassault Systemes Simulia Corp., Providence, RI, USA, 2014.

[17] Seleš, K., Abaqus Code for a Residual Control Staggered Solution Scheme for the Phase-Field Modeling of Brittle Fracture. https://data.mendeley.com/datasets/p77tsyrbx2/3, Mendeley data (2018).

[18] Nguyen, T.T., Yvonnet, J., Zhu, Q.Z., Bornert, M., Chateau, C., A phase field method to simulate crack nucleation and propagation in strongly heterogeneous materials from direct imaging of their microstructure. *Engineering Fracture Mechanics*, 139, 18-39 (2015).

[19] Bourdin, B., Francfort, G.A., Marigo, J.J., Numerical experiments in revisited brittle fracture. *J. Mechanics and Physics of Solids*, 48(4), 797-826 (2000).

[20] Seleš, K., Jurčević, A., Tonković, Z., Sorić, J., Crack Propagation Prediction in Heterogeneous Microstructure using an Efficient Phase-Field Algorithm. *Theoretical and Applied Fracture Mechanics*, 100, 289-297, (2019).

[21] Molnar, G., Gravouil, A., 2D and 3D Abaqus implementation of a robust staggered phasefield solution for modeling brittle fracture. *Finite Elements in Analysis and Design*, 130, 27-38 (2017).